anomaly. During La Niña events, the effect will be the opposite, keeping the resulting negative rainfall anomaly smaller.

To summarize: The cross-correlation analysis shows that there is a strong correlation between MSLA and the time series for EOF2. This correlation coefficient is around 0.6 when there is a 6-month lag of the EOF-2 time series with respect to MSLA. This means that MSLA at Caldera can be used as a physical advisory parameter to forecast rainfall anomalies in the Central and Southern Regions of Chile. The 6-month lag tells us that there is a delay between the ocean responses to ENSO at Caldera that can help planning in advance to prevent or mitigate the effects of this phenomenon over the Chilean ecosystem.

Acknowledgments

We gratefully acknowledge the wisdom of Captain Carlos Bidart, Director of the Chilean Hydrographic and Oceanographic Service, to permit R.N. to visit Florida State University to perform this analysis. The NOAA Global Change Office provided the "sojourn expenses" for the visit. We thank Mike Hall, Jim Buizer, Ken Mooney, and Felix Espinoza for their insight in encouraging the cooperation.

This research is supported by NOAA TOGA Grant NA16RC0279-01.

Rodrigo H. Nuñez
Departamento de Oceanografía
Servicio Hidrográfico y Oceanográfico de la Armada
Errazuriz 232 Playa Ancha
Valparaíso, Chile
and
James J. O'Brien and Jay F. Shriver
Mesoscale Air-Sea Interaction Group
Florida State University
Tallahassee, Florida 32306-3041, U.S.A.

Zonal Surface Current Distribution in the Tropical Indian Ocean from the XBT TOGA Network

Since the beginning of the TOGA program, XBT coverage of the Indian Ocean has been gradually extended by Australia (CSIRO) and France (ORSTOM) over the following routes (Figure 1): Fremantle - Sunda Strait (since 1983); Red Sea - Reunion Island (since 1985); Fremantle - Red Sea (since 1986); Fremantle - Persian Gulf (since 1986); Red Sea - Singapore (since 1987); and Reunion Island - Singapore (since 1990).

The first three routes provide roughly meridional sections in the band 20°S to 12°N with equatorial crossings at 55°E and 70°E. A third crossing is represented by the northern end of the line to Sunda Strait, which is near 7°S on the eastern boundary of the Indian Ocean and, as such, is representative of the equatorial thermocline near 98°E due to Kelvin wave adjustments. The last three routes have not been sampled as consistently or for as long a period as the first three. This report is a preliminary survey of the major geostrophic currents inferred from the XBT data and their seasonal variation, using only the first three lines. The results are also compared to earlier studies.

XBTs provide temperature profiles from the surface to 450 m (or more) about every 60 miles along the routes. Bi-monthly average values of SST, depth of the 20°C isotherm, and dynamic height relative to 400 db have been computed in bins of 1 degree of latitude in order to study qualitatively the zonal current distribution during a standard year. Dynamic height was calculated using the climatological temperature/salinity relationship.

Slope of the Isotherms at the Equator

At the equator, due to the absence of the Coriolis force, the zonal slope of the thermocline could be related to the zonal component of the current at the thermocline level. In order to represent the thermocline, the 20°C isotherm has been selected, as done already by Quadfasel (1982).

The depth of the 20°C isotherm at the equator has been calculated bimonthly on the Red Sea - Reunion Island (55°E) and Red Sea - Fremantle (70°E) routes and with additional data (Figure 1) provided by the TOGA Subsurface Data Centre at 85°E and at 45°E where data are numerous enough. Moreover, since it is representative of the equatorial thermocline near 98°E due to Kelvin wave adjustments, the depth of the 20°C isotherm at the northern end of the Fremantle - Sunda route has been included also.

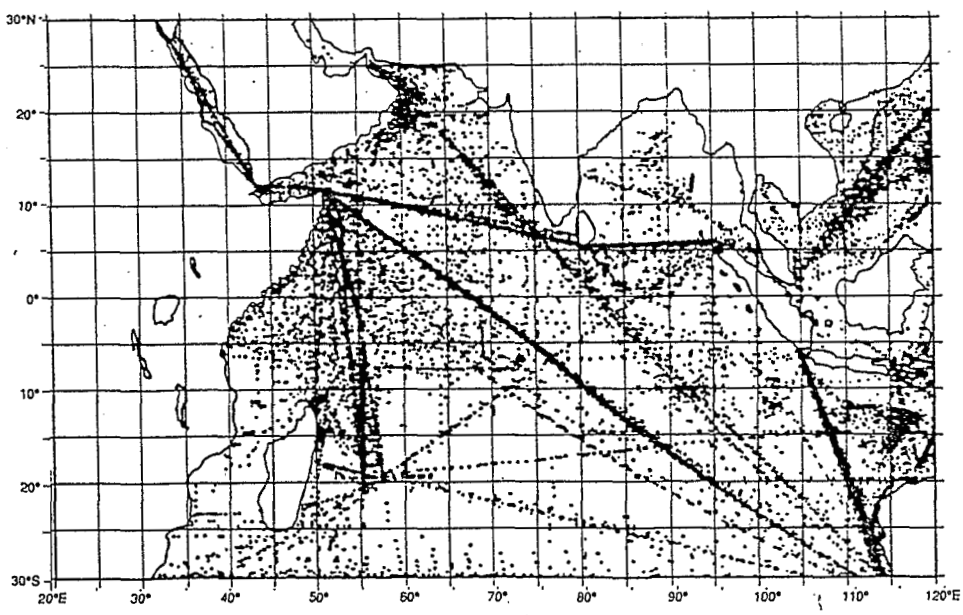

Figure 1. XBT data distribution from 1 January 1985 to 31 December 1990.

Figure 2 shows the depth of the 20°C isotherm from 100°E to 45°E. The slope reverses four times annually. From January to April, the 20°C isotherm is the deepest in the west and reaches 120 m, so that the slope is downward toward the west. From April to August, the 20°C isotherm is the deepest in the east (120 m), and the slope is downward toward the east. From August to October, the 20°C isotherm is the deepest again in the west (120 m), and from October to January, it is the deepest in the east (120 m again). In summary, the slope is westward during the Northeast (NE) and Southwest (SW) Monsoons and eastward during the transitions. Wyrtki (1971) also considered the 20°C isotherm depth and came to the same conclusions.

The zonal wind conditions (Sadler *et al.*, 1987) do not have a simple relationship to the equatorial slope. West of 65°E, the wind components are mainly meridional. East of 65°E, the zonal components are always eastward and consequently not connected with the reversal of the slope. The changes in slope apparently are a dynamic response to near-equatorial westerly winds east of 65°E during the transition seasons and may be influenced by the very strong monsoonal winds throughout the tropical zone.

The depth of the 20°C isotherm implies the presence of a heat pool in the western Indian Ocean during the NE and SW Monsoons. The heat pool moves to the eastern ocean during the transitions. This feature of the equatorial Indian Ocean is similar in some respects to the El Niño phenomenon.

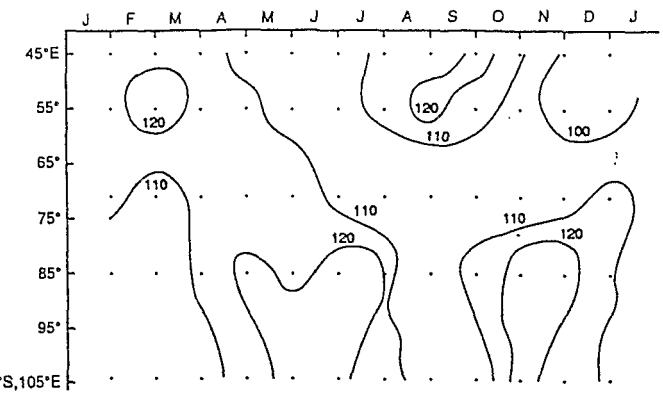

Figure 2. Depth of the 20°C isotherm along the equator. The data were averaged monthly in 2° latitude by 5° longitude bins centered at 45°E, 55°E, 70°E, and 85°E and smoothed with a running 2-month mean. The data at 7°S, 105°E are representative of the equator at 98°E.

Tropical Zonal Currents (20°S-10°N)

The meridional profiles of dynamic height (0/400 db) along the three main XBT routes are shown in Figure 3. They are used to describe the strength and direction of the major currents during the peak monsoons (February/March and August/September) and the transitions (May/June and November/December). The two lines to the Red Sea in the western Indian Ocean cover the latitude band 20°S to 12°N, while the Fremantle - Sunda Strait route extends northward only to 8°S. Figures 4, 5, 6, and 8 schematically illustrate the open-ocean currents inferred from the XBT data, and suggest how they are connected to the coastal currents off Africa.

February/March: This period is the time of the NE Monsoon. The monsoon induces a current toward the southwest along the African coast that carries salty water in the surface layer originating from the Arabian Sea (Donguy, 1974). In Figure 3, the XBT lines leading to the Red Sea show westward currents from 4°S to 6°N feeding the coastal current; this flow is the North Equatorial Current, the northern side of the Monsoon counterclockwise gyre (Wyrtki, 1973a), during the Asian Winter Monsoon. Eastward currents flow away from the boundary in the latitude band 12°S-4°S, with a stronger current on the western side of the basin. This is the South Equatorial Countercurrent, the southern side of the Monsoon gyre in this season. From approximately 16°S to 10°S, the South Equatorial Current flows westward (Figures 3 and 4). The lines on the eastern side of the basin show eastward flow south of 16°S, indicating the subtropical gyre of the South Indian Ocean.

The large-scale current pattern inferred from the XBT data is also in agreement with the results of the drifting buoys in the same area (Molinari et al. 1990) including some details. Molinari *et al.* point out that in March (at the end of the Northeast Monsoon), there is a northeastward coastal current north of 4°N, and this feature could be consistent with the presence of an eastward current north of 5°N on the XBT tracks (Figure 3). The results of a model (Woodberry *et al.*, 1989) also show eastward flow north of 5°N in agreement with the observations on the XBT tracks, and they are also in good agreement for January in the southwestern areas. The North Equatorial Current flowing westward on both sides of the equator is consistent with the atlas of Wyrtki (1971) and follows the slope of the 20°C isotherm.

May/June: This is a period of transition. The salty water from the Arabian Sea still persists north of 5°N (Donguy, 1974). The Monsoon gyre north of the equator still flows westward toward the coast of Somalia, but has weakened in the central ocean (Figures 3 and 5). The southern side of the gyre, the South Equatorial Countercurrent, has strengthened and on the western side of the ocean has shifted closer to the equator and merged with the transition jets (Wyrtki, 1973b). South of 5°S, a clockwise gyre is formed by the westward South Equatorial Current and the eastward South Equatorial Countercurrent. The eastward current flows all the way across the ocean and at the eastern boundary is deflected southeastward by the coast of Sumatra, so that it appears on the Fremantle - Sunda track near 8°S.

The large-scale pattern is very close to the February/March pattern, except for the current on the equator. In the equatorial area, the profile of dynamic height (Figure 3) is flat, and consequently the current is weak and the direction is uncertain; Molinari *et al.* (1990) point out a strong eastward equatorial current (equatorial jet) in May and June. On the other hand, the model of Woodberry *et al.* (1989) shows a weak westward current on the equator during April. In the west, on the Red Sea - La Reunion track, the energetic eddy system north of 4°N (Figure 3) is perhaps an indication of the Great Whirl (Duing *et al.*, 1980).

August/September: This is the period of the SW Monsoon. Warm and low-salinity water is carried eastward and northward along the coast of Somalia (Donguy, 1974). The

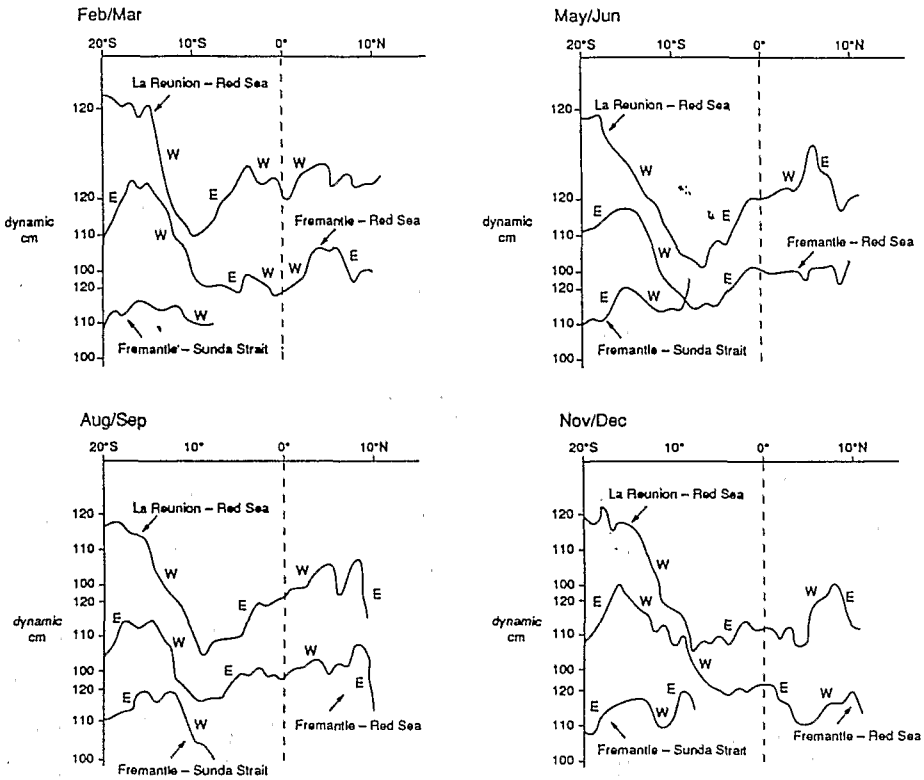

Figure 3. Surface dynamic height in dynamic centimeters along the XBT routes of the Indian Ocean.

South Equatorial Current appears to have strengthened, especially on the Sunda line, since February/March (Figures 3 and 6) and feeds the western boundary current. The current near and north of the equator to 5°N is also westward and feeds the boundary current. This observation of westward flow north of the equator does not agree with Wyrtki's (1973a) description of eastward surface currents throughout the Arabian Sea as far south as the equator, which is based on ship drift data and represents the surface current. Dynamic heights from XBTs represent the subsurface geostrophic flow. The difference is probably due to a real vertical shear in the currents, with directly wind-driven currents toward the east at the surface and persistence of the North Equatorial Current toward the west in the depth range of the thermocline (Figure 7). The South Equatorial Countercurrent is still evident in the western and central parts of the basin, although it has weakened since January/February.

Similar to the XBT analysis, the model of Woodberry *et al.* (1989) shows westward flow on the equator in July and the presence of several strong equatorial eddies in the west. The study by Molinari *et al.* (1990) did not have enough data to characterize the equatorial current. In the west, two eddies at 5°N and 8°N in the XBT analysis are in agreement with currents found near the Red Sea by Duing *et al.* (1980).

November/December: This transition time is characterized by the beginning of the southward advection of the salty water along the African coast (Donguy, 1974). The SW Monsoon gyre has shifted southward. A new counterclockwise gyre now appears north of the equator that could be considered the beginning of the NE Monsoon gyre. Eastward currents prevail on each side of the equator (the Wyrtki jet), more intensely on the north side. Reflection of the jet at the eastern boundary along the coast of Sumatra is seen on the Sunda track. South of the equator, the current pattern is almost the same as during the other seasons, except that the South Equatorial Countercurrent is weaker than in any of the preceding maps (Figures 3 and 8).

According to Molinari *et al.* (1990), a strong eastward jet on the equator also is obvious from the results of the drifting buoys, in agreement with this study. The Great Whirl is recognizable at 8°N in the western part of the ocean in both studies.

Discussion

The current pattern defined for each season is not exactly in agreement with Wyrtki (1971, 1973a). From surface drift, Wyrtki (1973a) defines two kinds of monsoon gyres that extend north of the equator: (1) prevailing during the NE Monsoon there is a counterclockwise gyre that includes the monsoon current along the Coast of Africa, the South Equatorial Countercurrent, and the North Equatorial Current; (2) during the SW Monsoon the gyre is clockwise and includes the monsoon current, the North Equatorial Countercurrent, and the South Equatorial Current. During the NE Monsoon the equatorial current is westward; during the SW Monsoon it is eastward. It is difficult to recognize (Figures 4 and 6) such gyres in the geostrophic current patterns obtained from the XBT data. As explained before, this discrepancy probably is due to the kinds of data utilized with wind drift affecting the surface flow in the ship-drift data discussed by Wyrtki (1973a).

For February/March, the current at the equator determined from the XBT data is westward, consistent with the Wyrtki (1971, 1973a) data. For August/September, the current determined from the XBT data is rather weak and of indeterminate direction, whereas the ship-drift data of Wyrtki (1971, 1973a) show a clear eastward current.

On the other hand, the current pattern defined for each season is almost in agreement with the results of the drifting buoys (Molinari *et al.*, 1990). However, the currents from drifting buoys typically seem stronger than the ones evaluated from dynamic heights. This discrepancy probably is due to the fact that the dynamic heights have been monthly averaged and consequently smoothed. That is particularly obvious in November/December at the time of the equatorial eastward jet. Moreover, this study gives interesting information about the eddies located in the Somali Current and crossed

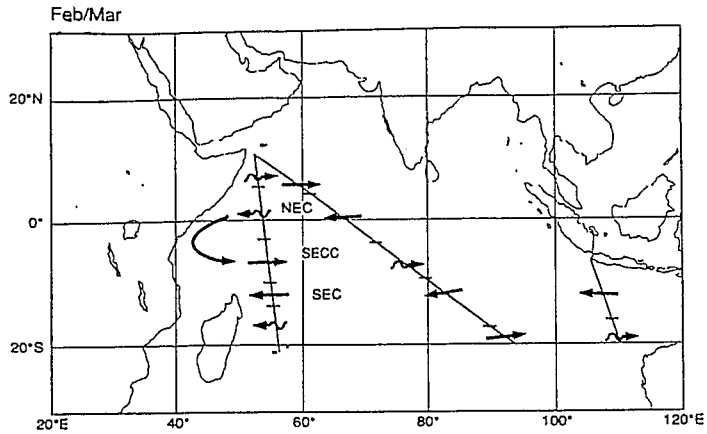

Figure 4. Qualitative zonal current evaluated for dynamic height slopes for February/March. The wavy arrow represents weak current.

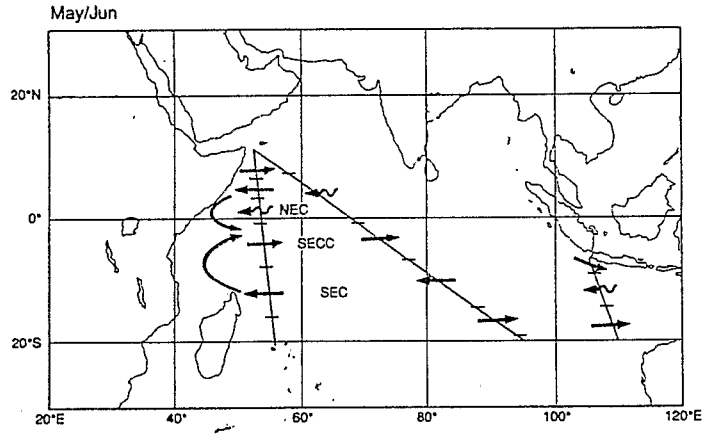

Figure 5. Same as Figure 4 except for May/June.

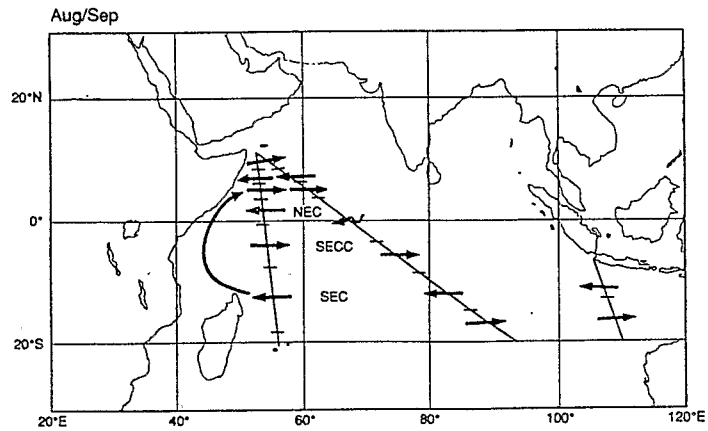

Figure 6. Same as Figure 4 except for August/September.

by the Red Sea - La Reunion route. Swallow and Fieux (1982) recorded when two eddies or only one appeared. Dynamic heights in May/June present only one eddy centered at 6°N (Figure 3) In August/September, two eddies are obvious, one centered at 5°N, the other centered at 8°N. In November/December, only one eddy appears. It is centered at 8°N and is much wider than in May/June. It is probably the Great Whirl identified in earlier studies.

This report is a preliminary assessment of material being prepared for a complete report on the seasonal thermal structure, dynamic height, and geostrophic transport for all of the TOGA XBT lines in the Indian Ocean.

Acknowledgments

R. Bailey is the scientist in charge of the CSIRO XBT network. T. Worby was computer programmer for the data analysis and display. Their support is gratefully acknowledged.

References

Donguy, J.R., 1974: Une annee d'observations de surface dans la zone de monsoon de la partie occidentale de l'Ocean Indien. *Cah. ORSTOM, Ser. Oceanog.* 12, 2, 117-128.

Duing, W., R.L. Molinari, and J.C. Swallow, 1980: Somali Current: evolution of surface flow. *Science*, 209, 588-590.

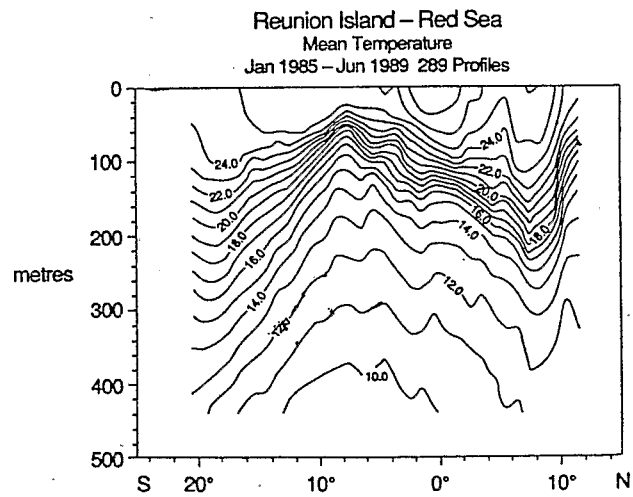

Figure 7. Mean temperature for August/September along La Reunion - Red Sea track.

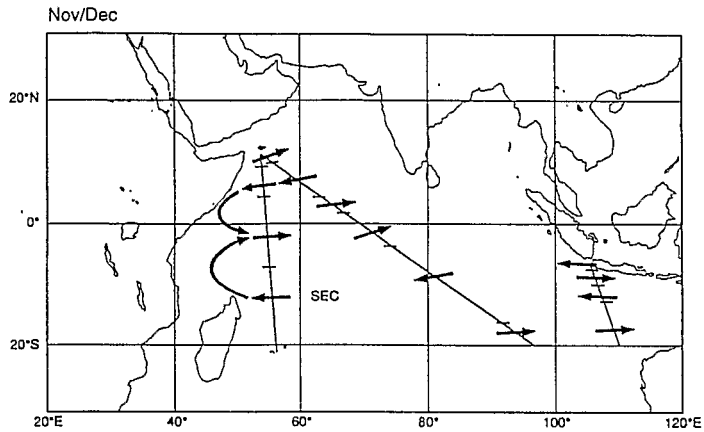

Figure 8. Same as Figure 4 except for November/December.

Molinari, R.L., D. Olson, and G. Reverdin, 1990: Surface current: distributions in the tropical Indian Ocean derived from compilations of surface buoy trajectories. *J. Geophys. Res.*, 95, 7217-7238.

Quadfasel, D.R., 1982: Low frequency variability of the 20°C isotherm topography in the western equatorial Indian Ocean. *J. Geophys. Res.*, 87, 1990-1996.

Swallow, J.C., and M. Fieux, 1982: Historical evidence for two gyres in the Somali Current. *J. Mar. Res.*, 40, Suppl., 747-755.

Woodberry, K.E., M.E. Luther, and J.J. O'Brien, 1989: The wind-driven seasonal circulation in the southern tropical Indian Ocean. *J. Geophys. Res.*, 94, 17,985-18,002.

Wyrtki, K., 1971: Oceanographic Atlas of the International Indian Ocean Expedition. National Science Foundation, Washington, D.C.

Wyrtki, K., 1973a: Physical oceanography of the Indian Ocean. In: *Ecological Studies. Analysis and Synthesis*, Vol. 3, Ed. by B. Zeitzchel, Springer-Verlag, Berlin, 18-36.

Wyrtki, K., 1973b: An equatorial jet in the Indian Ocean. *Science*, 181, 262-264.

J.Donguy
Centre ORSTOM de Brest
BP 70
29280 Plouzane, France
and
G. Meyers
CSIRO Division of Oceanography
GPO Box 1538
Hobart, Tasmania 7001, Australia

The Seasonal Cycle in a Coupled Ocean-Atmosphere Model

Introduction

In this note we discuss new results from a global coupled ocean-atmosphere model used to examine the behavior of the seasonal cycle of SST and wind stress in the tropics. There are several reasons why we believe that the seasonal cycle of SST should be studied. First, the seasonal cycle is the largest climate signal in the eastern tropical Pacific and tropical Atlantic Oceans. By getting the coupled model to accurately simulate the seasonal cycle, we therefore ensure that the physics governing the largest signal is included in the coupled models. Second, the seasonal cycle is not decoupled from interannual variability. For example, there appears to be phase-locking between the seasonal cycle and ENSO in the eastern Pacific (Rasmusson and Carpenter, 1982). Even those events that do not start warming in the eastern Pacific during the boreal spring, such as the 1982-83 event, terminate during the time when the eastern tropical Pacific climatologically cools. We therefore anticipate that it will be difficult to model ENSO variability without first correctly modeling the seasonal cycle. Finally, the seasonal cycle also may play a crucial role in limiting the predictability of climate variability. It has been noted that the Cane-Zebiak model has difficulty in making successful predictions across the boreal spring, when SST is warmest in the eastern tropical Pacific (Webster and Yang, 1992). It is important to determine if this barrier to predictability is an artifact of that particular anomaly prediction model or an inherent limitation to the predictability of the climate system.

Although a rudimentary understanding of the processes that govern the evolution of the coupled seasonal cycle is now beginning to emerge (Mitchell and Wallace, 1992; Bin Wang, 1992), a succinct description of the seasonal cycle of the Pacific ocean-atmosphere system has existed for over a decade (Horel, 1982). Horel describes the seasonal cycle of the tropical Pacific as reflecting significant coupled ocean-atmosphere interaction. In the northern extra-tropics, SST is warmest in the northern summer, and a similar phase relationship exists in the south-

TOGA Notes

Nova University
Oceanographic Center
8000 North Ocean Drive
Dania, Florida 33004, USA

JULY 1992

TOGA Notes

TOGA Notes is published quarterly by the Nova University Press. Its purpose is to provide a forum for presenting to the scientific community in a timely way new theories and findings on TOGA-related issues. Contributions will be published without charge and will not be copyrighted. Articles will be reviewed by the Science Editor, **Dr. Julian P. McCreary**, but, in the interest of time, will not be sent to outside referees for review. Most manuscripts will not be returned to authors for revision, provided that the articles are complete and otherwise suitable for publication. Permission to use scientific material contained in this bulletin must be obtained from the authors.

Manuscripts should be double-spaced, and figures must be camera-ready and suitable for reduction. References should be in the style of JAS/JPO and should be accurate, up-to-date, and complete. It should be noted that editors of refereed journals usually require that citations of bulletin articles be referenced as Personal Communication. A properly identified 5.25" floppy diskette (CP/M or MS-DOS), preferably in ASCII format, may accompany the manuscript. Authors are asked to provide complete mailing addresses; telephone, fax, and telex numbers; and e- mail addresses.

Manuscripts received within 6 weeks of a publication date, if accepted, will be included in that issue. Manuscripts should be submitted to the following address:

Ms. Jan Witte, Technical Editor
TOGA Notes
Nova University Oceanographic Center
8000 North Ocean Drive
Dania, Florida 33004, U.S.A.

Phone: (305) 920-1909; fax: 947-8559
e-Mail (Omnet): J.McCreary or J.Witte

Items concerning International TOGA Project Office (ITPO) planning or announcements should be sent to:

Mr. John Marsh, Director
ITPO, c/o WMO
Postal Box 2300
CH-1211 Geneva 2, Switzerland

Phone: 41 22 7308 225 (Director)
fax: 41 22 734 23 26; telex: 23260
e-Mail (Omnet): INTL.TOGA or V.Lee

CONTENTS